Thin Solid Films 561 (2014) 87–92

Contents lists available at ScienceDirect

Thin Solid Films

journal homepage: www.elsevier.com/locate/tsf

Effects of annealing on the compositional heterogeneity and structure in zirconium-based bulk metallic glass thin films

L. He [a], J.P. Chu [b], C.-L. Li [b], C.-M. Lee [b], Y.-C. Chen [b], P.K. Liaw [c], P.M. Voyles [a,*]

[a] Department of Materials Science and Engineering, University of Wisconsin-Madison, Madison, WI 53706, USA
[b] Department of Materials Science and Engineering, National Taiwan University of Science and Technology, Taipei 10607, Taiwan
[c] Department of Materials Science and Engineering, The University of Tennessee, Knoxville, TN 37996, USA

ARTICLE INFO

Available online 17 September 2013

Keywords:
Bulk metallic glass
Thin film metallic glass
Phase separation
Compositional fluctuation
Short-range order
Medium-range order
Fluctuation electron microscopy
Scanning transmission electron microscopy

ABSTRACT

In-situ heating fluctuation electron microscopy and scanning transmission electron microscopy have been utilized to study compositional and structural heterogeneities in $Zr_{51}Cu_{32}Al_9Ni_8$ thin films upon annealing. Composition fluctuations are present in the as-deposited thin films. Well below the glass transition temperature, the composition fluctuations increase with annealing time. Short- and medium-range order also change with annealing temperature. The observed heterogeneities in the glass structure persist until annealing causes crystallization. The 20 nm thick $Zr_{51}Cu_{32}Al_9Ni_8$ films contain oxide layers both at the surface and the film/substrate interface with the total thickness of 7–8 nm. In-situ annealing increased the oxygen content of the whole films to about 24 wt.% after 2 h at 400 °C.

1. Introduction

Amorphous phase separation, in which a parent amorphous phase separates into regions with two different compositions, has been observed in a variety of bulk metallic glasses, including $Pd_{80}Si_{20}$ [1], $Ni_{58.5}Nb_{20.25}Y_{21.25}$ [2], $Cu_{43}Zr_{43}Al_7Ag_7$ [3], and others [4]. In some cases, phase separation can have a desirable effect on the metallic glass properties. For example, the Zr–Cu–Al–Ni system contains several good glass forming alloys [5]. $Zr_{63.8}Cu_{15}Al_5Ni_{16.2}$ has high plasticity because it separates into regions of $Zr_{68.5}Cu_{8.1}Al_{2.1}Ni_{21.3}$ and $Zr_{62.4}Cu_{16.7}Al_{6.3}Ni_{14.6}$ with the length scale of 0.5–1 μm [6]. The phase separation is attributed to the positive enthalpy of mixing between Cu and Ni atoms and the negative enthalpy of mixing of Zr and Cu [7]. However the Ni-free glass $Cu_{47.5}Zr_{47.5}Al_5$ also separates into much smaller spherical regions 10–20 nm in diameter with different compositions from the matrix [8] and a tendency for Cu-rich regions 5–30 nm in diameter to form was reported in $Zr_{55}Cu_{30}Al_{10}Ni_5$ ingots annealed below the glass transition temperature, T_g [9].

We have investigated phase separation in sputtered $Zr_{51}Cu_{32}Al_9Ni_8$ thin films using in-situ heating in the scanning transmission electron microscope (STEM). Metallic glass thin films produced by vapor deposition effectively experience a much faster quench rate than melt-cast ingots or ribbons. Thus they may exhibit different phase separation behaviors. We show that $Zr_{51}Cu_{32}Al_9Ni_8$ films undergo composition fluctuations well below T_g. The composition fluctuations affect the short- and medium-range structures, and grow up to the point of crystallization.

2. Experimental procedures

20 nm thick $Zr_{51}Cu_{32}Al_9Ni_8$ thin films were sputtered onto silicon wafers, amorphous silicon and carbon TEM grids at 1.3 Å/s. The substrates were not intentionally heated during deposition. The magnetron sputtering method is described in [10]. The amorphous silicon TEM grids were SiMPore's UltraSM non-porous 5 nm amorphous silicon windows. The surface roughness specified by SiMPore is 0.3–0.4 nm root mean square. We have confirmed the absolute thickness fluctuations of ±0.7 nm from high angle annular dark field (HAADF) images [11]. The carbon grids on Mo supports were from Hummingbird Scientific. The carbon film is 15–25 nm thick.

Differential scanning calorimetry (DSC) measurements were conducted on $Zr_{51}Cu_{32}Al_9Ni_8$ films deposited on a glass substrate for about 10 h to a thickness of at least 8 μm. The film was removed from the substrate by lightly scratching it with tweezers, then tapping to remove the film. The resulting powder-like sample was measured in a NETZSCH 404 F3 DSC at a scan rate of 40 °C/min.

The STEM experiments were conducted at 200 kV using an FEI Titan S-Twin aberration-corrected STEM equipped with the EDAX X-ray energy dispersive spectroscopy (EDS) and Gatan GIF (ER865), and at 300 kV in an FEI TF30 Twin STEM with a GIF Tridiem. Compositional mapping at room temperature (RT) was performed in the FEI Titan using EDS spectrum imaging with a probe current of 390 pA, a semi-convergence angle of 24.5 mrad, and a pixel dwell time of 30 s. Electron energy loss spectroscopy (EELS) spectrum images were performed in a FEI TF30 STEM

* Corresponding author. Tel.: +1 608 265 6740.

0040-6090/$ – see front matter © 2013 Elsevier B.V. All rights reserved.
http://dx.doi.org/10.1016/j.tsf.2013.09.042

with a probe of 29 pA, a semi-convergence angle of 10.4 mrad, a semi-collection angle of 84.3 mrad, and a pixel dwell time of 0.04 s. Medium-range order was measured in the Titan using fluctuation electron microscopy (FEM) [12]. The FEM measurements were carried out with highly coherent electron probes of 1.5 nm in diameter and 1 mrad in semi-convergence angle. Electron nanodiffraction patterns from 1000 random selected sample areas were acquired to calculate one variance spectrum, V. V is defined by $V(k) = \langle I(k,\mathbf{r})^2\rangle_{\mathbf{r}} / \langle I(k,\mathbf{r})\rangle_{\mathbf{r}}^2 - 1$, where I is the electron diffraction intensity at a reciprocal space vector, k, and sample position, $\mathbf{r}$. $\langle\ \rangle$ indicates averaging over $\mathbf{r}$ [13]. The FEM data were collected with energy filtering and controlled coherence [14], corrected for Poisson noise, and filtering for constant sample thickness [11]. Short-range order was measured using selected area diffraction and FEM nanobeam diffraction.

In-situ heating was performed with a sample heating holder from Hummingbird Scientific. The heating and cooling rates were controlled at 20 °C/min. One sample was heated from 55 °C to 203 °C, cooled to RT at the end of one experiment session, then in a later experimental session, heated up to 355 °C and cooled to RT, then to 405 °C and cooled, and finally to 493 °C. The sample was annealed at each temperature for 1.5–2 h. FEM data was acquired at elevated temperatures. A separate sample was heated at 400 °C for a certain period of time, cooled to RT for EDS measurements, and was then heated up to a total of 2 h at 400 °C.

3. Results

The as-deposited 20 nm thick $Zr_{51}Cu_{32}Al_9Ni_8$ thin films on the Si support are uniformly amorphous, as shown in the TEM bright field image and electron diffraction pattern in Fig. 1(a). The electron diffraction pattern shows a diffuse first peak at 0.4 $Å^{-1}$. However, the high angle annular dark field (HAADF) image in Fig. 1(b) displays contrast at a spatial scale similar to or smaller than 1 nm. Some of the HAADF contrast may be due to surface roughness or oxidation, but the EDS analysis in Fig. 2 shows that there are composition fluctuations of all elements at the nanometer scale. Fig. 1(c) shows a cross-sectional TEM bright field image of a 20 nm $Zr_{51}Cu_{32}Al_9Ni_8$ thin film deposited onto a Si (001) substrate. The film consists of a surface layer, a main layer and a film/substrate interface layer, as shown in both TEM bright field image in Fig. 1(c) and the HAADF image in Fig. 1(d). The oxygen EELS spectrum image in Fig. 1(e) shows that oxygen is concentrated at the film surface and in the interface layer. Zirconium is more evenly distributed throughout the film as shown in Fig. 1(f). Thus, the $Zr_{51}Cu_{32}Al_9Ni_8$ films contain an approximately 3 nm thick surface oxide layer, 4 nm thick interface oxide layer, and 16 nm metal films.

Fig. 2(a) shows the similar HAADF contrast to Fig. 1(b). Fig. 2(b) shows the EDS composition maps from the area in (a), and Fig. 2(c) presents the Zr composition as a function of Cu composition for each pixel in the maps in Fig. 2(b). The Zr and Cu composition values are randomly distributed, but there is a nearly linear relationship between Zr and Cu compositions.

Fig. 3 shows the differential scanning calorimetry of a thick $Zr_{51}Cu_{32}Al_9Ni_8$ films grown on a glass slide. T_g = 479.6 °C and the crystallization temperature T_x = 511.8 °C. There is a small exothermic signal starting around 420 °C.

In-situ annealing of the $Zr_{51}Cu_{32}Al_9Ni_8$ films deposited on carbon grids at 400 °C (0.89 T_g) increased the composition fluctuations, as

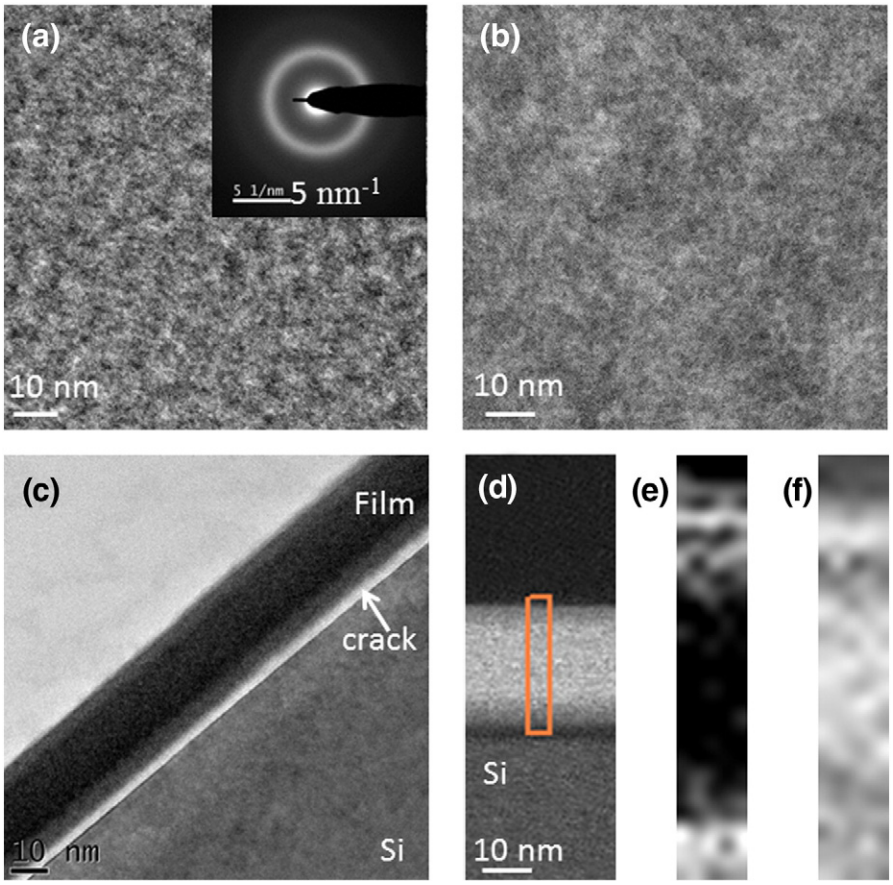

Fig. 1. As-deposited 20 nm thick $Zr_{51}Cu_{32}Al_9Ni_8$ films on amorphous Si thin film grids, plan-view (a–b) and on crystalline Si substrates, cross-sectional view (c–f). (a) Plan-view TEM bright field image. Inset is the electron diffraction pattern. (b) Plan-view HAADF image. (c) Cross-sectional bright field TEM image. The electron beam was parallel to the Si <110> axis. (d) Cross-sectional HAADF image. (e) Oxygen K edge EELS map (532 eV) from the orange window area in (d). (f) Zirconium $M_{4,5}$ edge EELS map (180 eV) from the orange window area in (d). The gray level in (e) and (f) is proportional to the EELS edge counts, with the brighter contrast representing the higher counts.